Diurnal Cycle of Shallow and Deep Convection for a Tropical Land and an Ocean Environment and Its Relationship to Synoptic Wind Regimes

L. GUSTAVO PEREIRA AND STEVEN A. RUTLEDGE

Department of Atmospheric Science, Colorado State University, Fort Collins, Colorado

(Manuscript received 14 September 2005, in final form 23 December 2005)

ABSTRACT

The characteristics of shallow and deep convection during the Tropical Rainfall Measuring Mission/Large-Scale Biosphere–Atmosphere Experiment in Amazonia (TRMM/LBA) and the Eastern Pacific Investigation of Climate Processes in the Coupled Ocean–Atmosphere System (EPIC) are evaluated in this study. Using high-quality radar data collected during these two tropical field experiments, the reflectivity profiles, rain rates, fraction of convective area, and fraction of rainfall volume in each region are examined. This study focuses on the diurnal cycle of shallow and deep convection for the identified wind regimes in both regions.

The easterly phase in TRMM/LBA and the northerly wind regime in EPIC were associated with the strongest convection, indicated by larger rain rates, higher reflectivities, and deeper convective cores compared to the westerly phase in TRMM/LBA and the southerly regime in EPIC. The diurnal cycle results indicated that convection initiates in the morning and peaks in the afternoon during TRMM/LBA, whereas in the east Pacific the diurnal cycle of convection is very dependent on the wind regime. Deep convection in the northerly regime peaks around midnight, nearly 6 h before its southerly regime counterpart. Moreover, the northerly regime of EPIC was dominated by convective rainfall, whereas the southerly regime was dominated by stratiform rainfall. The diurnal variability was more pronounced during TRMM/LBA than in EPIC. Shallow convection was associated with 10% and 3% of precipitation during TRMM/LBA and EPIC, respectively.

1. Introduction

The diurnal cycle is one of the most fundamental modes of climatic variability and the ability of any general circulation model to accurately represent the amplitude and the phase of this cycle over land and over ocean is a key test to the physical parameterizations in the model (Yang and Slingo 2001). Many studies have shown an afternoon peak in the diurnal cycle of convection over land that is linked to boundary layer destabilization caused by daytime insolation (Wallace 1975; Oki and Musiake 1994; Dai et al. 1999; Dai 2001). Several mechanisms have been proposed to explain the observed overnight enhancement in convection over the oceans (Gray and Jacobson 1977; Albright et al. 1985; Chen and Houze 1997; Hall and Vonder Haar 1999; Zuidema 2003). Gray and Jacobson (1977) proposed that convection over oceans was modulated by daily variations in the horizontal divergence field, which are generated by differential radiative heating between cloud-free areas and areas where convection is present. Another mechanism, discussed by Dudhia (1989), Tao et al. (1996), and Dai (2001), proposes that the overnight enhancement of convection over oceans is caused by a decrease in nighttime cloud entrainment due to the impacts of nighttime longwave cooling on relative humidities. Randall et al. (1991) concluded that the observed diurnal cycle over the oceans could be qualitatively accounted for by the direct radiation–convection interactions (i.e., daytime absorption of shortwave radiation by the upper portions of the convective clouds increases the static stability in cloudy regions and weakens vertical motions, while nighttime longwave cooling decreases the static stability and enhances convection). Nesbitt and Zipser (2003) made a comprehensive analysis of the diurnal cycle of rainfall using Tropical Rainfall Measuring Mission (TRMM) satellite measurements and also thoroughly reviewed the results of several studies that fo-

Corresponding author address: Gustavo Pereira, Department of Atmospheric Science, Colorado State University, Fort Collins, CO 80523-1374.
E-mail: gustavo@atmos.colostate.edu

cused on the diurnal cycle of convection over land and ocean in the Tropics.

Tropical precipitation falls from both convective and stratiform clouds. Convective precipitation is associated with strong vertical air motions, high rain rates, small horizontal dimension, intense radar echo, and areas where mass collection processes (i.e., coalescence and riming) are the dominant microphysical mechanisms for hydrometeor growth (Houze 1993; Schumacher and Houze 2003a). Shallow convection is associated with clouds with limited vertical development and involves the growth of small droplets by condensation, followed by the generation of larger drops by collision and coalescence. In the Tropics, cold cloud processes are typically observed when the cloud has significant vertical extent above the freezing level (Zipser and Lutz 1994). Hence, deep convection involves cold cloud processes such as aggregation, riming and deposition, though warm cloud processes may still operate in the above-freezing portions of these deep clouds. Precipitation from shallow clouds over the Tropics has been investigated in several studies using infrared (Petty 1999) and microwave satellite observations (Liu et al. 1995) and using TRMM's precipitation radar (Short and Nakamura 2000; Schumacher and Houze 2003b).

Several field campaigns in tropical land and tropical ocean environments, such as the Down Under Doppler and Electricity Experiment (DUNDEE), TRMM/Large-Scale Biosphere–Atmosphere Experiment in Amazonia (LBA), and the East Pacific Investigation of Climate Processes in the Coupled Ocean–Atmosphere System (EPIC), have identified alternating regional synoptic wind regimes that possess distinct thermodynamic and convective characteristics. It remains unknown how these alternating environmental conditions differentially impact the diurnal cycle of shallow and deep convective clouds on tropical ocean and tropical land locations. Elucidating these impacts may help future studies to shed light on the quantitative and individual contributions of thermodynamics and microphysics in the development of convective clouds. This study will focus on the diurnal cycle of shallow and deep convective precipitation over a tropical land and a tropical ocean location and how these diurnal cycles are modulated by the synoptic wind regimes found in each region.

The southwest Amazon region has been shown to possess two distinct modes associated with the low-level wind circulation: easterly and westerly (Cifelli et al. 2002; Halverson et al. 2002; Petersen et al. 2002; Rickenbach et al. 2002). Larger (smaller) raindrops (Tokay et al. 2002), larger (smaller) convective available potential energy (CAPE) and convection inhibition (CIN) values (Cifelli et al. 2002; Halverson et al. 2002; Cifelli et al. 2004), higher (lower) ratios of convective precipitation (Rickenbach et al. 2002), higher (lower) cloud condensation nuclei (CCN) concentrations, and increased (decreased) occurrence of lightning (Williams et al. 2002) are characteristics of the easterly (westerly) regime. In the easterly regime, the predominant pattern was the development of isolated convective cells, which grew up to become mesoscale convective systems with convective and stratiform precipitation, and the propagation of squall lines across the Amazon basin (Pereira Filho et al. 2002; Rickenbach 2004), which were occasionally associated with instability waves that formed in the northern coast of Brazil, near the state of Para (Greco et al. 1990; Cohen et al. 1995). The westerly regime was characterized by weaker convection, and the predominant mesoscale pattern was the occurrence of convective cells embedded in large stratiform regions. Rickenbach et al. (2002) showed that the westerly wind regime events during the TRMM/LBA were local manifestations of baroclinic wave influence on tropical latitudes during the summer, and are generated by a northwesterly flow along a stationary frontal zone that defines the South Atlantic convergence zone transporting moist air from the Amazon basin southeastward into the subtropics.

Another tropical area that has been shown to have convection modulated by synoptic variability is the east Pacific warm-pool region, where convective characteristics depend on the phase of easterly waves (Petersen et al. 2003): northerly regime (i.e., ahead of the easterly wave trough) and southerly regime (i.e., behind the easterly wave trough). Petersen et al. (2003) showed that the northerly regime was characterized by greater CAPE and reduced CIN values compared to the southerly regime. They also showed that vertical wind shear was strongest through the troposphere in the southerly regime, whereas the northerly phase was associated with more vertically developed convection and higher lightning flash rates.

2. Data and methodology

The TRMM/LBA was a major component of the National Aeronautics and Space Administration (NASA) TRMM ground validation effort. TRMM/LBA was conducted during the Amazonian wet season (Horel et al. 1989; Rao and Hada 1990), specifically during the months of January and February 1999 in the state of Rondonia, Brazil (Silva Dias et al. 2002). The area of intense measurements was located in the southwest portion of the Amazon between latitudes 9° and 13°S

and between longitudes 60° and 64°W. This region was covered by an extensive array of instruments, including multiple radiosonde and tethered balloon sites, a lightning detection network, rain gauge and disdrometer networks, a dual-wavelength profiler, surface observing stations, micrometeorological towers, sodars, surface radiation measurements, two Doppler radars [one C-band and one S-band radar with polarimetric capabilities (the S-Pol radar)] and two research aircraft, one of them carrying an X-band radar (Cifelli et al. 2002; Silva Dias et al. 2002).

The ITCZ component of EPIC took place in September and early October 2001, between the equator and 10°N along the 95°W meridian (Raymond et al. 2004). The observational platforms used in this campaign included the National Oceanic and Atmospheric Administration (NOAA) research vessel *Ronald H. Brown*, the National Science Foundation (NSF) research vessel *Horizon*, a NOAA P-3 aircraft, and the NSF/National Center for Atmospheric Research (NCAR) C-130 aircraft. The *Ronald H. Brown* was equipped with a C-band Doppler radar, a Doppler lidar, radiation instruments, rain gauges, a wind profiler, air–sea flux system, standard surface meteorological instrumentation, and also oceanographic instrumentation, including subsurface SST measurements. The first component of EPIC focused on the observation and understanding of the ocean–atmosphere processes responsible for the structure and evolution of the large-scale atmospheric heating gradients in the equatorial and northeastern Pacific portions of the cold tongue/ITCZ complex.

The TRMM/LBA radar dataset is composed of volume scans taken by the NCAR S-Pol 10-cm polarimetric radar between 11 January 1999 and 28 February 1999, totaling 6099 full volume scans (3123 in the easterly regime and 2976 in the westerly regime). Easterly and westerly regime periods were determined as in Petersen et al. (2002) using National Centers for Environmental Prediction (NCEP)–NCAR mean zonal winds at 850 hPa, calculated within a box corresponding to the TRMM/LBA region (7.5°–15°S, 68°–60°W). The EPIC dataset was obtained between 11 September 2001 and 1 October 2001 using the 5-cm Doppler radar on board the NOAA research vessel *Ronald H. Brown*, totaling 2981 full volume scans (1408 in the northerly regime and 1573 in the southerly regime). Data from 110 radiosonde profiles were used to identify the periods of northerly and southerly wind regimes. This identification of easterly wave phases was performed using a time series of 700-hPa meridional winds, which produced approximately three full easterly wave composites during the examined period. A description of the radars used in TRMM/LBA and EPIC are provided in Cifelli et al. (2002) and Petersen et al. (2003), respectively.

Reflectivity Z data obtained by radar volume scans in both field experiments (i.e., TRMM/LBA and EPIC) were interpolated to a Cartesian grid using a Cressman weighting function (Cressman 1959) with a radius of influence of 1.5 km in the horizontal and 1.0 km in the vertical. Reflectivity was interpolated to a domain of 101 by 101 horizontal grid points with 2-km grid spacing, and to 40 vertical levels with 0.5-km grid spacing.

A partitioning algorithm was used to discriminate between convective and stratiform precipitation, following Yuter and Houze (1997, 1998, hereafter called YH97–98). A more thorough description of how the partitioning algorithm works is found in appendix A. The classification was performed at the 2-km level and only for grid points with reflectivities exceeding 15 dBZ. Differences between convective and stratiform precipitation are more tenuous in weaker echoes and, thus, are more prone to misclassification. These areas of weaker reflectivities were left unclassified and were not used in any of the statistics presented in this study. Though we realize that suppressing the weak echoes could potentially impact our shallow convection statistics, we believe that our shallow convection statistics are mostly represented by medium-sized clouds transitioning from *cumulus mediocris* to *cumulus congestus* phase (because of their larger horizontal and vertical dimensions). Moreover, a sensitivity test, shown in appendix B, indicated that applying the classification scheme to weak echoes did not significantly change our shallow convection statistics. The algorithm's absolute (or intensity) threshold was set to 40 dBZ following previous studies such as Steiner et al. (1995), DeMott (1998a,b), Rickenbach and Rutledge (1998), Biggerstaff and Listemaa (2000), Cifelli et al. (2002), and Petersen et al. (2003). The parameters a and b used by the algorithm's gradient criterion vary from radar to radar according to calibration and resolution differences and they could be adjusted for an optimized performance in each region. However, we favored the use of a single set of parameters for the partition methodology instead of two sets of optimized parameters in order to maintain consistency in the regional intercomparison performed in this study. Hence, the parameters a and b were kept the same as YH97–98 (8 and 64 respectively). Several preliminary partition maps (not shown) were obtained and compared against their corresponding reflectivity maps to provide a subjective evaluation of algorithm performance using this set of parameters. We found that the algorithm performed well in both regions (i.e., TRMM/LBA and EPIC), in all wind regimes (i.e., east-

erly, westerly, northerly, and southerly) and for a variety of echo conditions, such as isolated, organized and embedded convection, and widespread stratiform precipitation.

Rain rates were obtained using two distinct Z–R relationships. The first relationship, shown in Eq. (1), was calculated using TRMM/LBA data (Carey and Rutledge 2000), while the second relationship, shown in Eq. (2), was calculated using aircraft data collected during EPIC (R. Cifelli 2002, personal communication):

$$Z = 465R^{1.08}\ (\text{mm}^6\ \text{m}^{-3}), \quad (1)$$

$$Z = 218R^{1.6}\ (\text{mm}^6\ \text{m}^{-3}). \quad (2)$$

The relationships shown in Eqs. (1) and (2) suggest that the average drop size distributions between TRMM/LBA and EPIC are quite different (with a higher contribution of smaller droplets to rainfall in the EPIC region), consistent with their continental and maritime locations, respectively.

To gain insight into the microphysical processes leading to precipitation in these two regions, convective precipitation was separated into two groups according to the location of the radar echo top relative to the 0°C level: shallow and deep. Therefore, shallow will refer to convection dominated by warm-phase processes (described in the introduction), while deep convection will refer to clouds where solid phase precipitation is also significant. Radar echo top information was used to determine if a cloud has grown past the freezing level. Rawinsonde temperature profiles during TRMM/LBA and EPIC indicated that the freezing level in these tropical regions was found between 4.5 and 5.5 km. Hence, a grid column that was classified as convective and in which the 5-dBZ echo top was found at or below 5.5 km was deemed *shallow* (a sensitivity test to this height threshold is also presented in appendix B), otherwise the convection was tagged as *deep*. Precipitation produced by stratiform grid points was not classified as either shallow or deep. Any references hereafter to total precipitation represent the sum of convective and stratiform precipitation. In addition, "convective precipitation" will refer to the sum of precipitation from shallow and deep convection.

The impacts of synoptic forcing on the diurnal cycle of precipitation can be evaluated by determining the contributions of shallow convection, deep convection, and stratiform areas to the spatial coverage and intensity of total precipitation. Therefore, four fractions were calculated for each volume scan: deep-convective-to-total echo area, deep-convective-to-total rainfall, shallow-convective-to-total echo area, and shallow-convective-to-total rainfall. Each of these four fractions

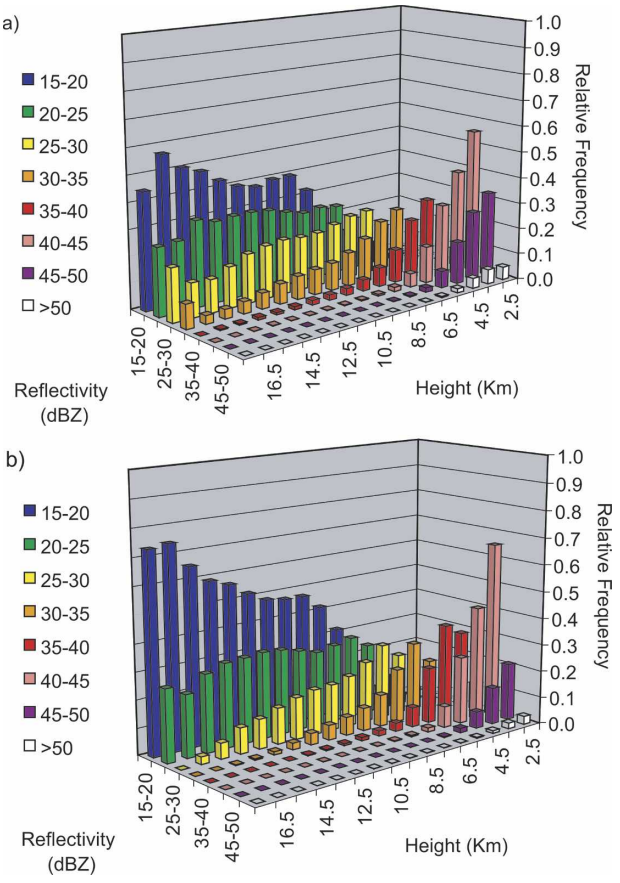

FIG. 1. PDFs, for different vertical levels, of radar reflectivities in convective areas during TRMM/LBA: (a) easterly regime and (b) westerly regime.

was calculated hourly, for each wind regime, and interpreted using a 3-h moving average. The same statistical methodology was used to calculate average convective echo top heights for each wind regime. In addition, probability distribution functions of radar reflectivity in convective areas were obtained. Rainfall fractions and rainfall cumulative distribution functions were computed using the Z–R relationships shown in Eqs. (1) and (2) for each of the two regions studied here. We applied the same Z–R relationships for shallow versus deep convective precipitation.

3. Results and discussion

a. TRMM/LBA

Figures 1a and 1b present reflectivity probability distribution functions (PDFs) of convective clouds during the easterly and westerly regimes, respectively, from the TRMM/LBA field project. There are two striking differences between these two distributions: 1) reflec-

TABLE 1. Mean environmental thermodynamic properties for different wind regimes of TRMM/LBA and EPIC.

	TRMM/LBA		EPIC	
Wind regime	Easterly	Westerly	Northerly	Southerly
CAPE (J)	1522	989	1865	1450
CIN (J)	−25	−13	−8	−9
Equilibrium level (mb)	150	155	149	162

tivities in the 25–30- and 30–35-dBZ ranges are more common at upper levels (i.e., above 8 km) during the easterly regime; 2) the easterly regime has more than one-third of reflectivities greater than 45 dBZ in the lowest 4 km, while in the westerly regime the same reflectivities represent less than one-fourth of occurrences at those heights. These results indicate that convective clouds in the easterly regime are more intense and vertically developed compared to those in the westerly regime; however, intense shallow clouds in the easterly regime could also be contributing to these differences. This is consistent with larger CAPE and CIN values in the easterly regime, as shown in Table 1.

Figure 2 shows average convective echo tops for the easterly and westerly regimes of TRMM/LBA as a function of local time (UTC − 4 h). The lowest echo top heights are observed a few hours after sunrise in both regimes, while the highest echo top heights are observed in the late afternoon and evening periods. In general, echo top heights in the easterly regime are 1 km higher than echo tops in the westerly regime, consistent with the reflectivity PDFs previously discussed. In addition, the 30-dBZ average echo top height reaches 6 km during the easterly regime, whereas in the westerly regime it does not extend beyond 5 km. The presence of 30-dBZ echo top heights above the freezing level (i.e., 5 km) is often associated with lightning production and presumably larger supercooled water and ice contents (Zipser 1994; Petersen et al. 1996). Thus, these results suggest that convective clouds in the easterly regime would be expected to have greater lightning flash rates than convective clouds in the westerly. Indeed, Petersen et al. (2002) and Williams et al. (2002) found greater lightning flash rates during easterly regime periods.

Rain-rate statistics are presented in Fig. 3. This figure subdivides these rain-rate statistics into those generated by shallow convective clouds and by deep convective clouds. During the easterly regime the 75th and 90th percentile of all convective rain rates (not shown) are found, respectively, at 29 and 60 (22 and 42) mm h^{-1} during the easterly (westerly) regime. Moreover, the 90th percentile of rain rates shows that the most intense

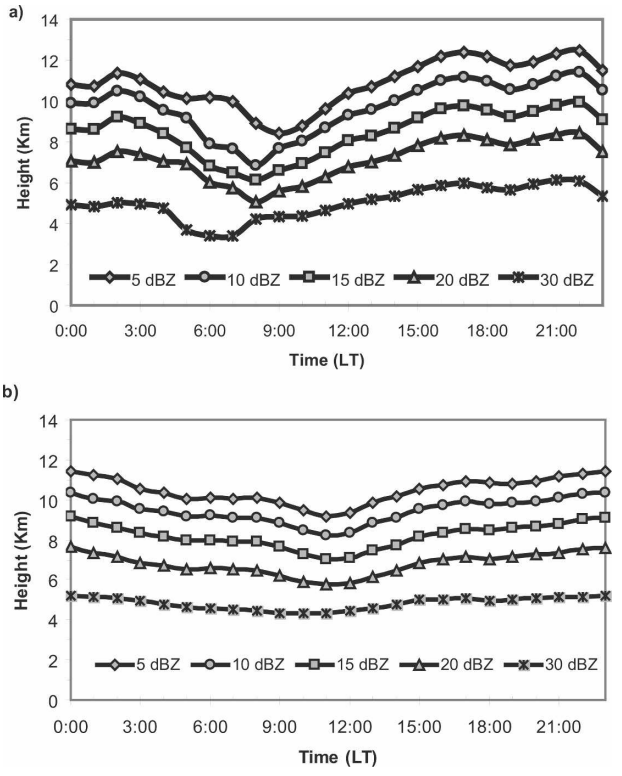

FIG. 2. Three-hour moving average of hourly echo top heights in convective areas during TRMM/LBA: (a) easterly regime and (b) westerly regime.

convective clouds in the easterly regime precipitate at significantly greater rates compared to the most intense convective echoes in the westerly regime. Cifelli et al. (2002) and Rickenbach et al. (2002) also observed more intense rain rates during the easterly regime in TRMM/LBA. When convection is separated into shallow and deep clouds, the cumulative distribution functions shown in Fig. 3a indicate that larger convective rain rates are found in both shallow and deep convective echoes in the easterly regime compared to their westerly regime counterparts. The 90th percentile of shallow and deep convective rain rates for the easterly (westerly) regime is, respectively, near 41 and 60 (29 and 43) mm h^{-1}. In fact, this percentile of rain rates produced by shallow convective clouds in the easterly regime is approximately equal to the same percentile of rain rates produced by deep convective clouds in the westerly regime. Hence, shallow convective cells in the easterly regime can produce rain rates similar to those found in deep convective cells in the westerly regime. Figure 3b shows that these intense shallow cells of the easterly regime tend to occur in the late afternoon, nearly at the same time as the peak rain rates of deep convective cells. Figure 3b also indicates a pronounced

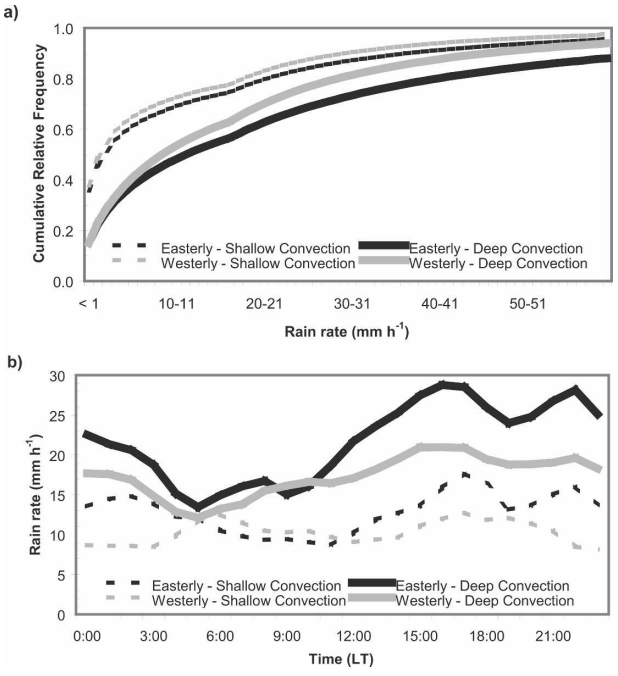

FIG. 3. Rain rates in shallow convective and deep convective precipitating systems during TRMM/LBA: (a) cumulative distribution function of rain rates and (b) 3-h moving average of hourly rain rates.

diurnal cycle of deep convective rain rates in both wind regimes, with the lowest (highest) average rain rates observed in the morning (late afternoon). Table 2 shows diurnally averaged rain-rate statistics. Table 2 indicates that, overall, the strongest (weakest) convective rain rates occur in deep (shallow) cells in the easterly (westerly) regime. Furthermore, the rain rates in the easterly phase convective cells are approximately 35% larger than their westerly phase counterparts.

Area and rainfall volume fractions are analyzed in Fig. 4 in order to gauge the magnitude of rainfall proportions. The statistics on rainfall volume fraction combine the information on the relative horizontal extent of systems (i.e., the area fraction) and the intensity of precipitation (i.e., rain rate). A prominent diurnal cycle is observed (Fig. 4a) with the greatest convective rainfall fractions observed around 1600 LT, at which time convective rainfall contributes nearly 90% (75%) of the total rain in the easterly (westerly) regime. The smallest convective rainfall fractions are observed just before sunrise, when the fraction of rainfall volume associated with convective areas is less than 10% (25%) in the easterly (westerly) regime. The rainfall volume fractions produced by shallow convective cells in TRMM/LBA are greatest in the late morning and early afternoon hours. The reason for this fraction to peak earlier than their rain rates (Fig. 3) is that the relative area of

TABLE 2. Average rain rate for all convective areas, shallow convective areas, and deep convective areas during the different wind regimes of TRMM/LBA.

	Avg rain rate (mm h^{-1})		
Wind regime	All convection	Shallow convection	Deep convection
Easterly	22.5	13.2	25.2
Westerly	16.6	10.5	18.5

these shallow convective cells decreases during the afternoon, owing to the increase in number and size of deep convective cells (Fig. 4b). In addition Figs. 4a and 4b also show a secondary maximum in convective fractions at 2200 LT during the easterly regime. This secondary maximum is absent in the westerly regime, suggesting that squall lines generated by instability waves that form in the northern coast of Brazil and propagate inland (Greco et al. 1990; Cohen et al. 1995), affecting the TRMM/LBA region during the easterly regime (Pereira Filho et al. 2002; Rickenbach 2004), could explain this feature. Figure 5a shows that more than half of all precipitation in the easterly (westerly) regime occurs between 1300 and 1700 (1200 and 1800) LT. The precipitation associated with shallow convection, shown in Fig. 5b, peaks between 1300 and 1400 LT in

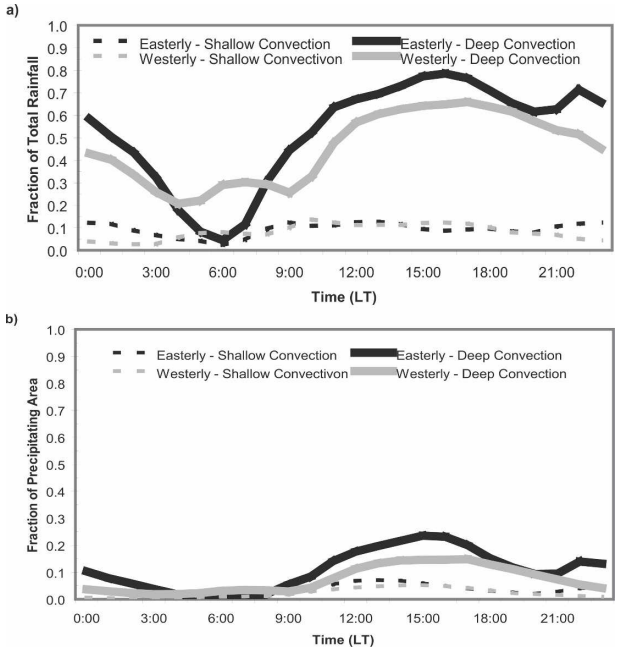

FIG. 4. Three-hour moving average of hourly fractions of shallow convective and deep convective precipitating systems during TRMM/LBA: (a) fraction of total rainfall and (b) fraction of precipitating area.

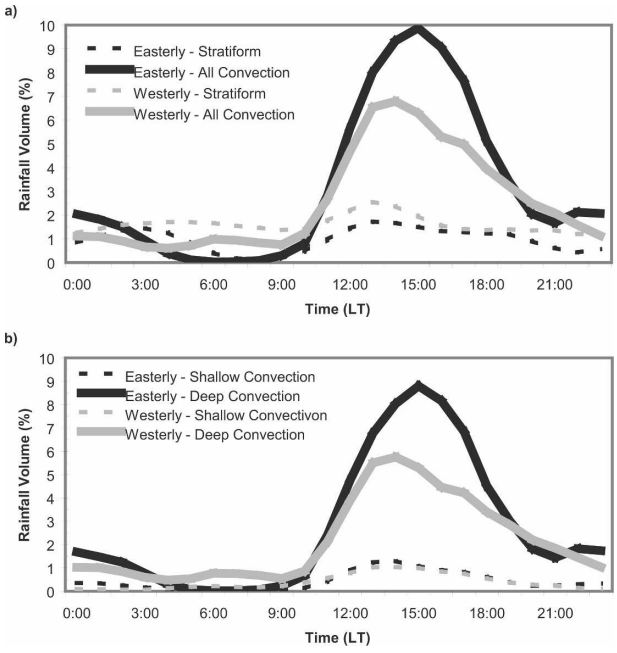

FIG. 5. Three-hour moving average of hourly rainfall volume contributions to total rainfall volume for each wind regime of TRMM/LBA: (a) stratiform and convective percentage contributions and (b) shallow convective and deep convective contributions.

both wind regimes, whereas precipitation associated with deep convective cells peaks at 1500 LT in the easterly regime, about one hour later than their westerly regime counterparts. Figure 5b also shows that the sharp increase in deep convective rainfall associated with the diurnal cycle does not start until 1000 LT. Therefore, the easterly regime's fast increase in deep convective rainfall fractions after 0700 LT, shown in Fig. 4a, is not an indication that the diurnal cycle of convective precipitation begins at that time, but rather is explained by the rapid decrease in stratiform precipitation, and by the small amount of total precipitation that occurs between 0600 and 0900 LT (usually less than 1% of the daily amount) during the easterly regime.

The average shallow convective area and rainfall volume fractions for the entire day during easterly and westerly regimes are shown in Table 3. Greater average convective (stratiform) area and rainfall volume fractions occur in the easterly (westerly) regime compared to the opposite wind regime over a 24-h period. The area covered by deep cells dominates the remaining area fraction associated with convection. Through the course of a day, more than 80% (90%) of the precipitating area had stratiform characteristics during the easterly (westerly) regime. The remaining precipitation area associated with convection is dominated by deep convective cells, which represent 75% or more of the convective area, at any given period of the day, in both wind regimes of TRMM/LBA. Despite the larger area associated with stratiform precipitation, the rainfall volume fractions associated with deep convection are significantly larger than their stratiform counterparts due to the larger rain rates associated with convective cells. During the course of a day, 77% (62%) of the rainfall is associated with convective clouds in the easterly (westerly) regime. Rickenbach et al. (2002) found somewhat lower convective rain fractions in the same region: 66% and 49% in the easterly and westerly regimes, respectively. The bulk of this convective precipitation is produced by deep convection, with just 10% (9%) of the total rainfall fraction associated with shallow convective cells in the easterly (westerly) regime. Rickenbach and Rutledge (1998) found that approximately 12% of the precipitation was associated with sub-mesoscale-convective-system-scale, nonlinear cells in the west Pacific warm-pool region during the Tropical Ocean and Global Atmosphere Program's Coupled Ocean–Atmosphere Response Experiment (TOGA COARE), while Simpson et al. (1993) found that isolated convective cells produced less than 10% of the observed rainfall in the Maritime Continent region near Darwin, Australia.

b. EPIC

Figure 6 shows that convective systems during EPIC, like TRMM/LBA, had significant differences in the frequency of intense reflectivities (i.e., greater than 45 dBZ) at low levels between the northerly and southerly wind regimes. The cores of northerly regime convective cells are twice more likely to attain reflectivities greater

TABLE 3. Average area and rainfall fractions of total precipitation during the different wind regimes of TRMM/LBA.

	Avg fraction of precipitating area (%)			Avg fraction of tot rainfall (%)		
Wind regime	Stratiform	Shallow convection	Deep convection	Stratiform	Shallow convection	Deep convection
Easterly	83	4	13	23	10	67
Westerly	91	2	7	38	9	53

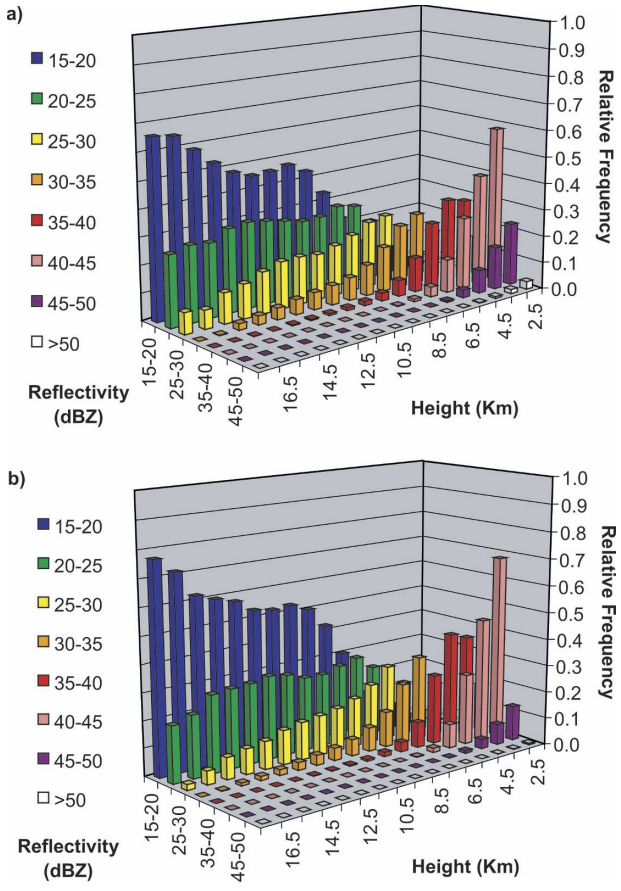

FIG. 6. PDFs, for different vertical levels, of radar reflectivities in convective areas during EPIC: (a) northerly regime and (b) southerly regime.

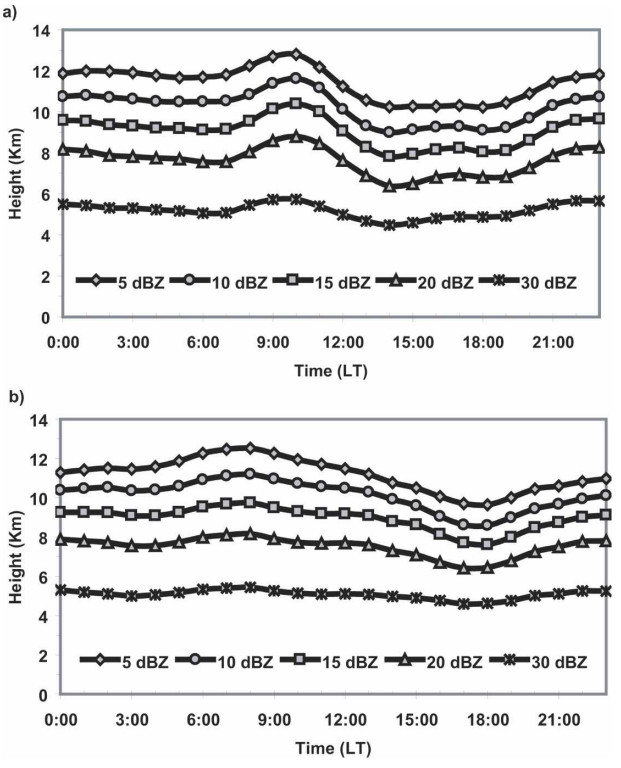

FIG. 7. Three-hour moving average of hourly echo top heights of convective areas during EPIC: (a) northerly regime and (b) southerly regime.

than 45 dBZ than southerly regime convective cells. Figure 6 also shows differences between northerly and southerly wind regimes as to the vertical extent of the convective cores. Although such differences are not as strong as those observed between easterly and westerly regimes of TRMM/LBA, the EPIC convective cores tend to be slightly more vertically developed during the northerly regime. Thus, the results shown here suggest a tendency for convection in the northerly regime to be more intense than in the southerly regime, consistent with Petersen et al. (2003).

For EPIC the average echo top heights, shown in Fig. 7, are usually highest during the morning period in both wind regimes, while the lowest echo top heights usually occur in the late afternoon and early evening. Several explanations have been given as the cause for convection to be less intense in the afternoon over oceanic regions such as EPIC. One of these explanations includes the nighttime increase of relative humidities due to longwave radiational cooling and, consequently, a reduction in entrainment and enhanced cloud development (Dudhia 1989; Tao et al. 1996; Dai 2001). Another explanation associates the modulation of convection to the differential radiative heating between convective and cloud-free regions, which produces a daily variation in the horizontal divergence field (Gray and Jacobson 1977). Figure 7 also shows that echo top heights in the northerly regime tend to be slightly higher than in the southerly regime, except during early morning and early afternoon periods when southerly regime average echo tops are up to 1 km higher than echo tops in the northerly regime. Nevertheless, when time of day is disregarded, the difference in echo top heights between the two regimes is insignificant.

In the northerly regime of EPIC the 75% (90%) percentile of rain rates is found near 15 (24) mm h^{-1}, whereas in the southerly regime this percentile is found at 13 (19) mm h^{-1}. Consequently, the gap between the northerly and southerly convective rain rates observed in Fig. 8a increases at higher percentiles. This indicates that high rain rates are more frequently observed in the northerly regime. The largest differences are observed between 10 and 35 mm h^{-1}, which correspond to reflectivities between 39 and 48 dBZ. Figure 8a also shows that the 75th percentile of shallow convective

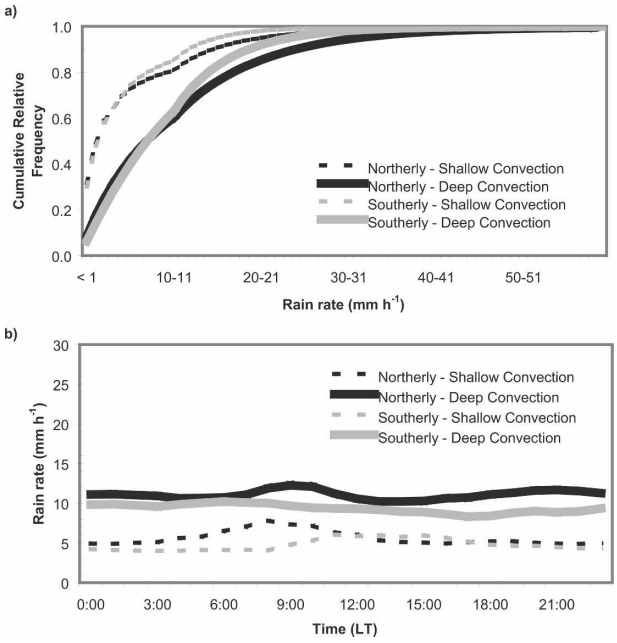

FIG. 8. Rain rates in shallow convective and deep convective precipitating systems during EPIC: (a) cumulative distribution function of rain rates and (b) 3-h moving average of hourly rain rates.

rain rates is the same for both regimes (4 mm h^{-1}) and the 90th percentile is slightly higher in the northerly regime (12 mm h^{-1}) compared to the southerly regime (10 mm h^{-1}). The cumulative distribution function (CDF) for deep convective cells is nearly identical to the CDF for all convective cells due to their higher frequency of occurrence of when compared to shallow convective cells. Figure 8b shows that there is little diurnal variation in the intensity of deep convective rain rates, particularly in the southerly regime, but they tend to peak around 0900 LT in the northerly regime. However, average shallow rain rates significantly increase in the morning and peak around 0800 LT during the northerly regime, while during the southerly regime the increase is less pronounced and achieves a peak around noon. Table 4 indicates that the average rain rates for shallow and deep convective cells in the northerly (southerly) regime are, respectively, 5.6 and 11.1 (4.7 and 9.6) mm h^{-1}.

Figure 9a shows a slight decreasing trend in convective rainfall fractions through the morning with a minimum in the afternoon hours. Both wind regimes show a tendency for the rainfall associated with deep convection to increase at night. Nonetheless, rainfall from stratiform clouds is responsible for the majority of the rain produced during the southerly regime, regardless of the time of day, and is also evidenced in Table 5. Deep, mixed-phase, convective cells produce over 90%

TABLE 4. Average rain rate for all convective areas, shallow convective areas, and deep convective areas during the different wind regimes of EPIC.

	Avg rain rate (mm h^{-1})		
Wind regime	All convection	Shallow convection	Deep convection
Northerly	10.3	5.6	11.1
Southerly	9.1	4.7	9.6

of the convective rainfall in the EPIC region in both wind regimes. Convective rainfall fractions are higher in the northerly regime. The fraction of total precipitation associated with stratiform features was found to be near 40% (60%) in the northerly (southerly) regime. These numbers are consistent with those retrieved by TRMM's precipitation radar (Schumacher and Houze 2003a). Contribution from shallow convective cells is less than 10% throughout the day and is highest at 0800 and 1800 LT. Figure 9b shows a similar diurnal variation of convective area fractions in the EPIC region. As in Fig. 9a, the diurnal cycle of rainfall fractions is most pronounced for deep convection in the northerly regime. These fractions are generally small throughout the day and are lowest in the afternoon. Table 5 shows that the total convective area fraction obtained for the northerly regime (20%) is larger than that obtained for

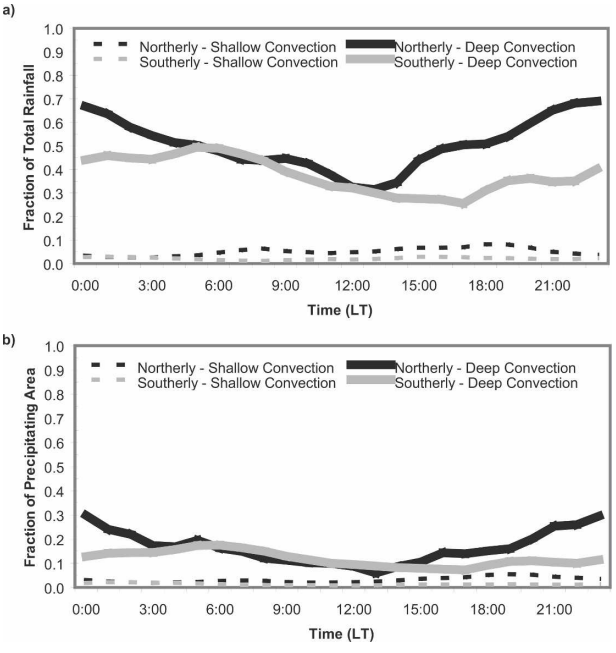

FIG. 9. Three-hour moving average of hourly fractions of shallow convective and deep convective precipitating systems during EPIC: (a) fraction of total rainfall and (b) fraction of precipitating area.

TABLE 5. Average area and rainfall fractions of total precipitation during the different wind regimes of EPIC.

	Avg fraction of precipitating area (%)			Avg fraction of tot rainfall (%)		
Wind regime	Stratiform	Shallow convection	Deep convection	Stratiform	Shallow convection	Deep convection
Northerly	80	3	17	42	4	54
Southerly	86	1	13	59	2	39

the southerly regime (14%). Hence, the majority of precipitating areas in the EPIC region (i.e., 80% or more) are associated with stratiform echoes. The remaining precipitating area is associated mostly with deep convective cells. When averaged over the entire day, shallow, warm rain cells represent only 15% (7%) of the convective precipitating areas in the northerly (southerly) regime, but less than 3% (1%) of the total precipitation. Figure 10 clearly shows that the diurnal cycle of precipitation during EPIC was very different depending on the wind regime. In the northerly regime the convective (stratiform) rainfall volume begins to increase at 1400 (2100) LT and peaks around 0100 (0400) LT. During most of the day convective rainfall contributes more to the total rainfall than its stratiform counterpart. In contrast, the southerly regime presents a diurnal cycle of convective (stratiform) rainfall that begins around 1700 (0000) LT and peaks around 0700 (0800) LT. Furthermore, the contribution of stratiform rainfall to the total rainfall volume in the southerly regime is equal to or greater than the contribution of convective rainfall.

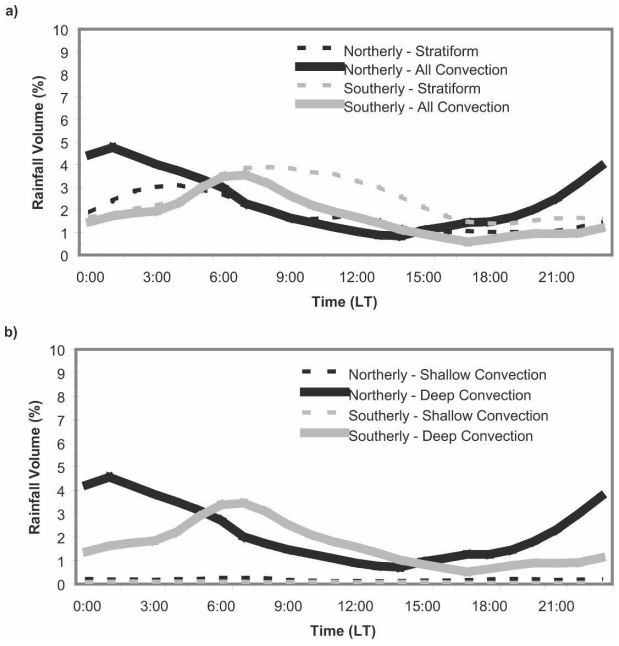

FIG. 10. Three-hour moving average of hourly rainfall volume contributions to total rainfall volume for each wind regime of EPIC: (a) stratiform and convective percentage contributions and (b) shallow convective and deep convective contributions.

4. Summary and conclusions

Radar data collected during the TRMM/LBA and EPIC field campaigns were examined to determine the impacts of different thermodynamic conditions, associated with alternating wind regimes, on the diurnal cycle of shallow and deep convective precipitation in a tropical land and a tropical ocean environment. The results shown in this study provide a quantitative characterization of the diurnal cycle of these convective systems during the TRMM/LBA and EPIC. Analyses used in this study included reflectivity profiles, average echo top heights, rain rates, fractions of convective area, and rainfall contribution from shallow and deep convective cells and stratiform clouds.

In general, convection during the easterly regime of TRMM/LBA tended to more frequently possess characteristics associated with vertically developed clouds: higher reflectivities at the lower levels, greater echo top heights, greater rain rates, and larger convective area and rainfall fractions. These characteristics were also more common during the northerly regime (i.e., pretrough) of EPIC, compared to the southerly regime (i.e., post-trough). These results are consistent with previous studies such as Cifelli et al. (2002), Halverson et al. (2002), Petersen et al. (2002), Rickenbach et al. (2002), Petersen et al. (2003), and Cifelli et al. (2004), but our study extends these findings over the course of the diurnal cycle and examines how different wind regimes (and their associated thermodynamic environments) affect shallow and deep convective systems. Overall, the convection in TRMM/LBA was more intense compared to the EPIC region, consistent with expected differences in continental versus oceanic location. Noteworthy is the spread of average rain rates produced by deep convective cells when all four wind regimes are compared, with the highest value observed in the easterly regime of TRMM/LBA (25.2 mm h^{-1}) and the lowest value observed in EPIC's southerly re-

gime (9.6 mm h^{-1}). Higher average rain rates would still be observed in TRMM/LBA even if the same Z–R relationship had been used in both regions. This reflects the more energetic convection over the tropical land masses associated with higher CAPE and resultant larger vertical velocities.

Average echo top heights were shown to be highest in the TRMM/LBA easterly regime, followed by the EPIC northerly and southerly regimes, while the lowest echo tops occurred in the TRMM/LBA westerly regime. While echo tops in the northerly and southerly regimes were similar, it is obvious that echo tops in the TRMM/LBA easterly and westerly regime were very different. Higher tropopause heights in TRMM/LBA coupled with larger values of CAPE in the easterly phase could possibly explain the greater vertical development of clouds in the easterly regime. The average profile of rawinsonde temperatures and dewpoint temperatures (not shown) during TRMM/LBA indicated that the tropopause was usually in the vicinity of 85 mb (or 17.5 km), whereas in the EPIC region the tropopause was typically found near 120 mb (or 15.5 km). Moreover, the different thermodynamic profiles observed in each region, as evidenced by their different combinations of CAPE and CIN values shown in Table 1, play a role in the determination of the vertical extent of convective clouds.

Noteworthy is the observed higher rain rates in the westerly regime of TRMM/LBA compared to both wind regimes of EPIC since the former was shown to be associated with weaker reflectivity profiles. Intense convective rain rates (i.e., greater than 60 mm h^{-1}) occur more frequently in the TRMM/LBA region. This would be the case even if the same *Z–R* relationship were used in both regions. The light rain rates observed in the CDFs presented in this study are generally associated with the lower-reflectivity areas that surround the core of convective cells, and are classified as convective by the partitioning algorithm for being within the radius of a convective center. Instantaneous, intense rain rates are more common in shallow, warm convective clouds over the TRMM/LBA region compared to the deep convective clouds in the EPIC region, owing to the expected high precipitation efficiencies in the former cloud type.

The fraction of convective rainfall contributed by shallow convective cells was greater during TRMM/LBA (~10%) than in EPIC (~3%). EPIC results are consistent with the results obtained during Global Atmospheric Research Programme (GARP) Atlantic Tropical Experiment (GATE) by Cheng and Houze (1979), who found that convective clouds less than 5 km in depth (i.e., shallow convective cells) were associated with a very small portion (~2%) of the rainfall. The EPIC fraction is closer to the values obtained by Rickenbach and Rutledge (1998), who found that 3% of the total rainfall over the TOGA COARE was associated with shallow, warm rain-dominated cells. According to the results presented here, in both regions of this study, over 85% of the convective rainfall was produced by deeper convective features involving mixed-phase processes. The fraction of stratiform rainfall is 59% in the southerly regime, whereas in the other three regimes this fraction is less than 43%. The thermodynamic profile of the environment during the southerly regime yields the lowest equilibrium level. The highest fraction of convective area is observed in the northerly regime (20%). The high CAPE, low CIN combination of the environment in the northerly regime may act to allow convective energy to dissipate into numerous, less intense convective elements. In the easterly regime the CAPE is still high, but CIN is 3 times larger than in the northerly regime. This combination is likely to be more favorable for the development of fewer, but deeper and more intense, convective cells. This explains why the average fraction of precipitating area associated with convection is larger in the easterly regime compared to the northerly regime.

Although the distinct thermodynamic conditions observed in each wind regime of our tropical land site have significant impacts on the intensity of deep convection and on its contribution to total precipitation, there is little change in the phase of the diurnal cycle between wind regimes. Convection during TRMM/LBA underwent a pronounced diurnal cycle that initiated in the late morning and peaked in the afternoon during both wind regimes. In contrast, the oceanic environment of EPIC yielded diurnal cycles of convection that markedly vary in intensity and also in phase depending on the wind regime. The northerly regime is dominated by convective precipitation and has a diurnal cycle that initiates earlier in the afternoon and peaked around 0100 LT, whereas the southerly regime is dominated by stratiform precipitation and possesses a diurnal cycle that initiates near sunset and peaks near sunrise. Although the mechanisms for the convective overnight enhancement over oceans are not well understood, the significance of stratiform rain areas during the afternoon in the southerly regime may hinder and delay the initiation of convective processes. In addition to that, the northerly regime's thermodynamic environment, as indicated by the CAPE and CIN values shown in Table 1, is more conducive to convective development compared to the southerly regime. Therefore, the varying atmospheric buoyancy conditions associated with changes in synoptic-scale winds appear to have a

TABLE B1. Sensitivity test results for the average area and rainfall fractions of total precipitation as a function of the minimum reflectivity threshold used to partition the radar data.

Region	Min Z threshold	Avg fraction of precipitating area (%)			Avg fraction of tot rainfall (%)		
		Stratiform	Shallow convection	Deep convection	Stratiform	Shallow convection	Deep convection
LBA	5 dBZ	90	4	6	31	11	58
	15 dBZ	87	3	10	30	10	60
EPIC	5 dBZ	87	3	10	53	3	44
	15 dBZ	83	3	14	51	3	46

larger impact on the diurnal cycle of convection over the tropical ocean location compared to the tropical land site.

Acknowledgments. The authors would like to acknowledge Drs. Robert Cifelli and Stephen Nesbitt for their valuable discussions and all the personnel involved in the TRMM/LBA and EPIC data collection efforts. TRMM/LBA was supported by the National Aeronautics and Space Administration and the National Science Foundation. The National Oceanic and Atmospheric Administration and the National Science Foundation supported EPIC. This research was funded by the NSF Grant ATM-0002256 from the Large-scale Dynamic Meteorology Program, NASA TRMM Grant NAG5 4754, and NOAA Grant NA17RJ1228.

APPENDIX A

Partitioning Algorithm

The partitioning algorithm assigns the convective/stratiform classification to grid points using two criteria. The first criterion is known as the absolute or intensity criterion. If the reflectivity in a grid point exceeds a set threshold (40 dBZ in this study), the grid point is assigned the convective classification. The grid points that do not have reflectivities exceeding this threshold are submitted to a second test known as the gradient or peakedness criterion. After this test, a grid point will also receive the convective classification if the reflectivity at that grid point exceeds the parameter ΔZ, which is defined as

$$\Delta Z = a \cos\left(\frac{\pi Z_{\text{bg}}}{2b}\right). \quad \text{(A1)}$$

Therefore DZ depends on two fixed parameters, a and b (8 and 64 were used in this study, respectively), and on the variable Z_{bg}, which represents the background reflectivity. The background reflectivity is calculated for each grid point and is defined as the average reflectivity within an 11-km radius of the grid point being classified. Only positive reflectivity values are used to calculate this average. Once both criteria have been applied to all grid points, the algorithm then defines a convective radius around each of these convective grid points. All grid points that are found to be within the radius of one of these convective grid points are also assigned a convective classification. The size of the convective radius varies from 1 to 5 km and is a function of the background reflectivity Z_{bg}.

APPENDIX B

Sensitivity Tests

A sensitivity test was performed in order to analyze the impacts of our decision to not partition weak echoes and use that data in our statistics. Area and rain fractions for stratiform, shallow convection, and deep convection were calculated using a minimum threshold of 5 and 15 dBZ (the setting used in this study). The results of this sensitivity test are presented in Table B1 . The lower minimum threshold had a larger impact in the area fractions compared to the rain fractions and this impact was also more obvious in the TRMM/LBA region. Nevertheless, the impacts were rather small in all fractions, particularly in the shallow convection fractions. The largest changes occurred in the area fractions of deep convection, which decreased by 4% in both TRMM/LBA and EPIC, and were mostly associated with the increase of stratiform precipitating areas.

Another sensitivity test was performed to evaluate how our rain and area fraction results changed if the maximum height definition of shallow convection was changed. These fractions were calculated using three different height thresholds (using 5-dBZ echo top height) to separate shallow from deep convection: 4.5, 5.0, and 5.5 km (the latter being the definition we used in this paper). A summary of the results is presented in Table B2. Stratiform fractions were obviously not affected by changing this setting. Lowering the shallow/deep height threshold lowered the contribution of shallow convection to total rainfall and precipitating area,

TABLE B2. Sensitivity test results for the average area and rainfall fractions of total precipitation as a function of the definition used for the maximum echo top height of shallow convection.

Region	Shallow max height	Avg fraction of precipitating area (%)			Avg fraction of tot rainfall (%)		
		Stratiform	Shallow convection	Deep convection	Stratiform	Shallow convection	Deep convection
LBA	4.5 km	87	2	11	30	7	63
	5.0 km	87	3	10	30	9	61
	5.5 km	87	3	10	30	10	60
EPIC	4.5 km	83	2	15	51	1	48
	5.0 km	83	2	15	51	2	47
	5.5 km	83	3	14	51	3	46

as expected. The results of Table B2 show that rain fractions are more sensitive to the shallow/deep height threshold than the area fractions, but none of the fractions changed by more than 3%.

REFERENCES

Albright, M. D., E. R. Recker, R. J. Reed, and R. Dang, 1985: The diurnal variation of deep convection and inferred precipitation in the central tropical Pacific during January–February 1979. *Mon. Wea. Rev.,* **113,** 1663–1680.

Biggerstaff, M. I., and S. A. Listemaa, 2000: An improved scheme for convective/stratiform echo classification using radar reflectivity. *J. Appl. Meteor.,* **39,** 2129–2150.

Carey, L. D., and S. A. Rutledge, 2000: The relationship between precipitation and lightning in tropical island convection: A C-band polarimetric radar study. *Mon. Wea. Rev.,* **128,** 2687–2710.

Chen, S. S., and R. A. Houze Jr., 1997: Diurnal variation and life cycle of deep convective systems over the Pacific warm pool. *Quart. J. Roy. Meteor. Soc.,* **123,** 357–388.

Cheng, C.-P., and R. A. Houze Jr., 1979: The distribution of convective and mesoscale precipitation in GATE radar echo patterns. *Mon. Wea. Rev.,* **107,** 1370–1381.

Cifelli, R., W. A. Petersen, L. D. Carey, and S. A. Rutledge, 2002: Radar observations of the kinematic, microphysical and precipitation characteristics of two MCSs in TRMM-LBA. *J. Geophys. Res.,* **107,** 8077, doi:10.1029/2000JD000264.

——, L. Carey, W. A. Petersen, and S. A. Rutledge, 2004: An ensemble study of wet season convection in southwest Amazonia: Kinematics and implications for diabatic heating. *J. Climate,* **17,** 4107–4124.

Cohen, J. C. P., M. A. F. Silva Dias, and C. A. Nobre, 1995: Environmental conditions associated with Amazonian squall lines: A case study. *Mon. Wea. Rev.,* **123,** 3163–3174.

Cressman, G. P., 1959: An operational objective analysis system. *Mon. Wea. Rev.,* **87,** 367–374.

Dai, A., 2001: Global precipitation and thunderstorm frequencies. Part II: Diurnal variations. *J. Climate,* **14,** 1112–1128.

——, F. Giorgi, and K. E. Trenberth, 1999: Observed and model simulated precipitation diurnal cycle over the contiguous United States. *J. Geophys. Res.,* **104,** 6377–6402.

DeMott, C. A., and S. A. Rutledge, 1998a: The vertical structure of TOGA COARE convection. Part I: Radar echo distributions. *J. Atmos. Sci.,* **55,** 2730–2747.

——, and ——, 1998b: The vertical structure of TOGA COARE convection. Part II: Modulating influences and implications for diabatic heating. *J. Atmos. Sci.,* **55,** 2748–2762.

Dudhia, J., 1989: Numerical study of convection observed during the Winter Monsoon Experiment using a mesoscale two-dimensional model. *J. Atmos. Sci.,* **46,** 3077–3107.

Gray, W. M., and R. W. Jacobson Jr., 1977: Diurnal variation of deep cumulus convection. *Mon. Wea. Rev.,* **105,** 1171–1188.

Greco, S., and Coauthors, 1990: Rainfall and surface kinematic conditions over central Amazonia during ABLE 2B. *J. Geophys. Res.,* **93,** 17 001–17 014.

Hall, T. J., and T. H. Vonder Haar, 1999: The diurnal cycle of west Pacific deep convection and its relation to the special and temporal variation to tropical MCSs. *J. Atmos. Sci.,* **56,** 3401–3415.

Halverson, J. B., T. M. Rickenbach, B. Roy, H. Pierce, and E. Williams, 2002: Environmental characteristics of convective systems during TRMM-LBA. *Mon. Wea. Rev.,* **130,** 1493–1509.

Horel, J. D., A. N. Hahmann, and J. E. Geisler, 1989: An investigation of the annual cycle of convective activity over the tropical Americas. *J. Climate,* **2,** 1388–1403.

Houze, R. A., 1993: *Cloud Dynamics*. Academic Press, 573 pp.

Liu, G., J. A. Curry, and R.-S. Sheu, 1995: Classification of clouds over the western equatorial Pacific Ocean using combined infrared and microwave satellite data. *J. Geophys. Res.,* **100,** 13 811–13 826.

Nesbitt, S. W., and E. J. Zipser, 2003: The diurnal cycle of rainfall and convective intensity according to three years of TRMM measurements. *J. Climate,* **16,** 1456–1475.

Oki, T., and K. Musiake, 1994: Seasonal change of the diurnal cycle of precipitation over Japan and Malaysia. *J. Appl. Meteor.,* **33,** 1445–1463.

Pereira Filho, A. J., M. A. F. Silva Dias, R. I. Albrecht, L. G. Pereira, A. W. Gandu, O. Massambani, A. Tokay, and S. Rutledge, 2002: Multi-sensor analysis of a squall line in the Amazon region. *J. Geophys. Res.,* **107,** 8084, doi:10.1029/2000JD000305.

Petersen, W. A., S. A. Rutledge, and R. E. Orville, 1996: Cloud-to-ground lightning observation from TOGA COARE: Selected results and lightning location algorithms. *Mon. Wea. Rev.,* **124,** 602–620.

——, S. W. Nesbitt, R. J. Blakeslee, R. Cifelli, P. Hein, and S. A. Rutledge, 2002: TRMM observations of intraseasonal variability in convective regimes over the Amazon. *J. Climate,* **15,** 1278–1294.

——, R. Cifelli, D. J. Boccippio, S. A. Rutledge, and C. Fairall, 2003: Convection and easterly wave structure observed in the

eastern Pacific warm pool during EPIC-2001. *J. Atmos. Sci.,* **60,** 1754–1773.

Petty, G. W., 1999: Prevalence of precipitation from warm-topped clouds over eastern Asia and the western Pacific. *J. Climate,* **12,** 220–229.

Randall, D. A., Harshvardhan, and D. A. Dazlich, 1991: Diurnal variability of the hydrologic cycle in a general circulation model. *J. Atmos. Sci.,* **48,** 40–62.

Rao, V. B., and K. Hada, 1990: Characteristics of rainfall over Brazil: Annual variations and connections with the southern oscillation. *Theor. Appl. Climatol.,* **42,** 81–91.

Raymond, J. D., and Coauthors, 2004: EPIC2001 and the coupled ocean–atmosphere system of the tropical east Pacific. *Bull. Amer. Meteor. Soc.,* **85,** 1341–1354.

Rickenbach, T. M., 2004: Nocturnal cloud systems and the diurnal variation of clouds and rainfall in southwestern Amazonia. *Mon. Wea. Rev.,* **132,** 1201–1219.

——, and S. A. Rutledge, 1998: Convection in TOGA COARE: Horizontal scale, morphology, and rainfall production. *J. Atmos. Sci.,* **55,** 2715–2729.

——, R. Nieto Ferreira, J. B. Halverson, D. L. Herdies, and M. A. F. Silva Dias, 2002: Modulation of convection in the southwestern Amazon basin by extratropical stationary fronts. *J. Geophys. Res.,* **107,** 8040, doi:10.1029/2000JD000263.

Schumacher, C., and R. A. Houze Jr., 2003a: Stratiform rain in the Tropics as seen by the TRMM precipitation radar. *J. Climate,* **16,** 1739–1756.

——, and ——, 2003b: The TRMM precipitation radar's view of shallow, isolated rain. *J. Appl. Meteor.,* **42,** 1519–1524.

Short, D. A., and K. Nakamura, 2000: TRMM radar observations of shallow precipitation over the tropical oceans. *J. Climate,* **13,** 4107–4124.

Silva Dias, M. A. F., and Coauthors, 2002: Cloud and rain processes in a biosphere–atmosphere interaction context in the Amazon region. *J. Geophys. Res.,* **107,** 8072, doi:10.1029/001JD000335.

Simpson, J., T. D. Keenan, B. Ferrier, R. H. Simpson, and G. J. Holland, 1993: Cumulus mergers in the maritime continent region. *Meteor. Atmos. Phys.,* **51,** 73–99.

Steiner, M., R. A. Houze, and S. E. Yuter, 1995: Climatological characteristics of three-dimensional storm structure from operational radar and rain gauge data. *J. Appl. Meteor.,* **34,** 1978–2007.

Tao, W.-K., S. Lang, J. Simpson, C.-H. Sui, B. Ferrier, and M.-D. Chou, 1996: Mechanisms of cloud–radiation interaction in the Tropics and midlatitudes. *J. Atmos. Sci.,* **53,** 2624–2651.

Tokay, A., A. Kruger, W. Krajewski, and A. Pereira Filho, 2002: Measurements of drop size distribution in southwestern Amazon region. *J. Geophys. Res.,* **107,** 8052, doi:10.1029/2001JD000355.

Wallace, J. M., 1975: Diurnal variations in precipitation and thunderstorm frequency over the conterminous United States. *Mon. Wea. Rev.,* **103,** 406–419.

Williams, E. R., and Coauthors, 2002: Contrasting convective regimes over the Amazon: Implications for cloud-electrification. *J. Geophys. Res.,* **107,** 8082, doi:10.1029/2001JD000380.

Yang, G.-Y., and J. Slingo, 2001: The diurnal cycle in the Tropics. *Mon. Wea. Rev.,* **129,** 784–801.

Yuter, S. E., and R. A. House Jr., 1997: Measurements of raindrop size distributions over the Pacific warm pool and implications for *Z–R* relations. *J. Appl. Meteor.,* **36,** 847–867.

——, and ——, 1998: The natural variability of precipitating clouds over the western Pacific warm pool. *Quart. J. Roy. Meteor. Soc.,* **124,** 53–99.

Zipser, E. J., 1994: Deep cumulonimbus cloud systems in the Tropics with and without lightning. *Mon. Wea. Rev.,* **122,** 1837–1851.

——, and K. R. Lutz, 1994: The vertical profile of radar reflectivity of convective cells: A strong indicator of storm intensity and lightning probability? *Mon. Wea. Rev.,* **122,** 1751–1759.

Zuidema, P., 2003: Convective clouds over the Bay of Bengal. *Mon. Wea. Rev.,* **131,** 616–634.